Frequency characteristic analysis on acoustic emission of mortar using cement-based piezoelectric sensors

Youyuan Lu* and Zongjin Li

Department of Civil and Environmental Engineering, Hong Kong University of Science and Technology, Clear Water Bay, Hong Kong

Abstract. Acoustic emission (AE) monitoring was conducted for mortar specimens under three types of static loading patterns (cubic-splitting, direct-shear and pull-out). Each of the applied loading patterns was expected to produce a particular fracture process. Subsequently, the AEs generated by various fracture or damage processes carried specific information on temporal micro-crack behaviors of concrete for post analysis, which was represented in the form of detected AE signal characteristics. Among various available characteristics of acquired AE signals, frequency content was of great interest. In this study, cement-based piezoelectric sensor (as AE transducer) and home-programmed DEcLIN monitoring system were utilized for AE monitoring on mortar. The cement-based piezoelectric sensor demonstrated enhanced sensitivity and broad frequency domain response range after being embedded into mortar specimens. This broad band characteristic of cement-based piezoelectric sensor in frequency domain response benefited the analysis of frequency content of AE. Various evaluation methods were introduced and employed to clarify the variation characteristics of AE frequency content in each test. It was found that the variation behaviors of AE frequency content exhibited a close relationship with the applied loading processes during the tests.

Keywords: mortar; acoustic emission; cement-based piezoelectric sensor; frequency domain; energy; nondestructive testing.

1. Introduction

Various non-destructive testing (NDT) methods are available now for flaw or defect monitoring of materials. Among them, acoustic emission (AE) is an effective NDT method based on passive monitoring. In case of concrete, AEs can be generated when micro-cracks and macro-cracks form and propagate. Released fracture energy spreads in the form of elastic waves with a certain spatial distribution of amplitude and polarization of the motions that are related to corresponding crack modes (Ohtsu 1987). Normally, piezoelectric sensors shall be employed to possibly detect the AEs and transform them into electrical signals. The electrical signals can be fetched and extracted by followed data processing device to recognize its waveform character (Grosse *et al.* 2003). Based on signal-based analysis results, the crack or damage process of concrete structure can be interpreted and evaluated for early failure warning and life-time assessment (Carpinteri *et al.* 2007a,b).

Early research on the AE monitoring mostly relied on evaluation of traditional AE parameters (e.g., accumulated events number, event rate). Observed evident shift in measured parameters helped

---

*Corresponding Author, PhD candidate, E-mail: yylu@ust.hk

to effectively identify corresponding temporal fracture stages. And variations in micro-structural phenomena during concrete fracture processes are capable of being explicitly explained by AE parameter-based analysis (Li and Shah 1994, Landis 1999). Apart from elementary investigation on variations of AE parameters, many researches commenced to pay more attention on the characterization of AE of concrete. Given the physical analogy between seismology and AE, the behavior of concrete during fracture process can be interpreted (Ohtsu *et al.* 1991, Li 1996) by characteristic study similar to seismology. Hence, frequency domain analysis is considered as a promising aspect of characteristics study for AE signals from concrete cracks, and some preliminary work has been done on this issue (Maji and Sahu 1994, Daponte *et al.* 1995). Theoretically, the frequency content of AE ought to have a close relationship with the temporal condition of fracture in concrete. However, due to the limitation of the frequency response of traditional AE sensor and signal processing capability, the discussions on the frequency content are yet not sufficient.

In this study, embedded cement-based piezoelectric sensors have been used as transducers of AE monitoring system for the aim of monitoring fracture processes of concrete under various loading conditions. Its feature of broad band in frequency domain response makes the frequency content study of AE possible and feasible. The mostly reported frequency range of AE from concrete fracture and damage in literature can be covered by the employed sensors. The objective of this research is to investigate the characteristics of AEs in frequency domain during concrete fracture processes using information provided by improved AE monitoring system. By means of appropriate AE signal frequency content evaluation methods, frequency content variation tendencies were figured out for specified loading processes of the tests. Observed tendencies of AE frequency content variations indicate the shift of released AE energy from low frequency components to high frequency components with the increment of load levels. According to evaluation results, the frequency content characteristics of AE sources (i.e., micro-cracks of mortar) are considered closely related to temporal loading stages of mortar. The frequency analysis of AE provides a distinctive means of investigating fracture processes and micro-crack behaviors of mortar and concrete materials.

2. AE monitoring system (DEcLIN) details

2.1 Cement-based piezoelectric sensor

Broad band frequency domain response is one of the desired capabilities when an appropriate piezoelectric sensor for frequency analysis of AE is chosen. Normally, the available frequency domain response range of a piezoelectric sensor is determined by its acoustic properties and assorted data acquisition devices. As far as the frequency domain performance of employed piezoelectric sensor concerned, a good compatibility on acoustic properties and mechanical properties between sensor and matrix material can ensure the accurate and reliable broad band AE monitoring. In civil engineering, concrete is the most popular construction material. However, there exists relatively large difference on acoustic impedance and stiffness between concrete and traditional piezoelectric ceramic sensors.

In order to achieve better compatibility between sensing element and concrete matrix, issues stated previously have to be properly addressed. Li *et al.* developed a brand new cement-based piezoelectric composite (Li *et al.* 2002) that owns an acoustic impedance value (~10 Mrayls) quite close to that of the concrete matrix (~8.6 Mrayls), which ensures a minimum signal distortion and

Fig. 1 Cement-based piezoelectric sensor

maximum signal energy transmission efficiency. And it empowers the employed cement-based piezoelectric composite be able to exhibit electrical response to a very broad frequency components of AE from concrete cracks. Meanwhile, coupling issue could be properly solved by embedment of cement-based composite sensor into a concrete. Signal-to-noise ratio (SNR) could be enhanced accordingly to weaken the frequency content of background noise in detected AE. Up to now, piezoelectric composites with nine types of connectivity patterns have been fabricated and applied for sensor and actuator purposes (Akdogan *et al.* 2005). In this experiment, cement-based piezoelectric composite of 0-3 connectivity pattern (Qin *et al.* 2010) was employed to make piezoelectric sensor as shown in Fig. 1.
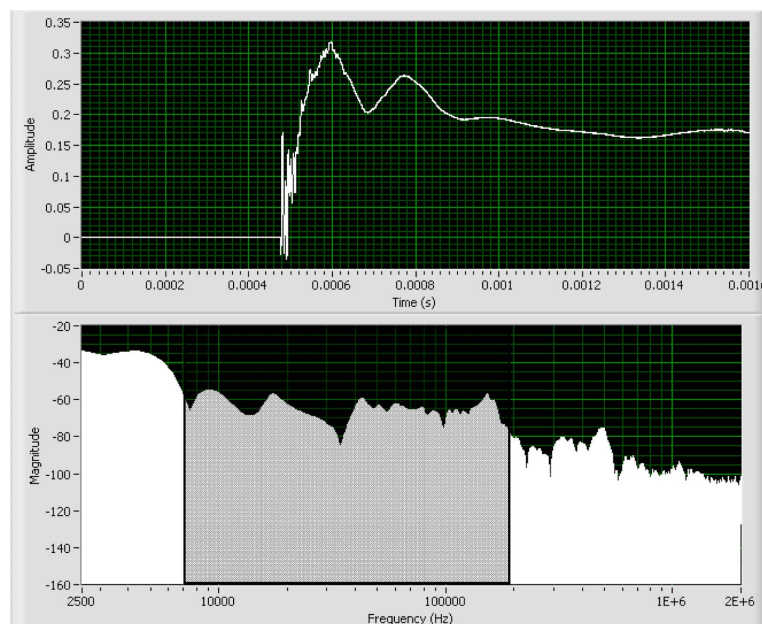

Fig. 2 Time and frequency domain response of cement-based piezoelectric sensor subjected to Hsu-Nielsen pencil lead break (The top graph is time domain, and the bottom graph is frequency domain. The flat frequency domain response region is highlighted by shadow)

The concrete matrix backed AE sensor calibration curve subjected to standard Hsu-Nielsen pencil lead break is illustrated in Fig. 2. This artificial acoustic source is frequently used to examine the useful frequency range of AE sensor employed. Herein, a flat frequency domain response $H(f)_{dB}$ covering required functional frequency region with relatively high sensitivity can be observed in Fig 2. Whereas, the fracture of pencil lead break will inevitably produce a stepwise displacement of the contact surface (Berthelot *et al*. 1992). Basically, the sensor surface, initially compressed by pencil lead, is suddenly released when the lead breaks, producing a localized stepwise displacement superimposed in the detected AE. Thus, the obtained frequency response owns an additive constant as Eq. (1).

$$|H(f)|_{dB} = |S(f)|_{dB} - 20\log(1/2\pi f) \tag{1}$$

Here, $H(f)$ is the obtained frequency response, while $S(f)$ is the real frequency response subjected to pencil lead break.

The superimposed constant value definitely won't result in invalidation of obtained frequency response if merely comparison study is necessary. Hence, we neglect the effect of $20\log(1/2\pi f)$ in this study. And totally eight piezoelectric sensors were embedded in each mortar specimen (see Fig 3, 5 and 7) to constitute the detecting array for AE monitoring on mortar specimens during loadings.

2.2 Home-programmed DEcLIN monitoring system

The elementary function blocks in DEcLIN AE monitoring system consist of cement-based piezoelectric sensors, voltage pre-amplifiers, 8-channel DAQ and corresponding functional software.

Broadband voltage pre-amplifiers (20 kHz ~ 1 MHz) are used to amplify the Micro-Volt scale acquired signals into Mill-Volt scale ones. An 8-channel 12 bit resolution DAQ is connected to the pre-amplifiers to simultaneously acquire real-time signal data. Sampling rate is set to be 5 MHz during the tests to satisfactorily cover the entire potential frequency range of AE signals. Distortion of acquired AE waveform is considered negligible. Therefore, information carried by frequency characteristics in AE signals will be preserved completely. The software is subdivided into two basic function components: signal acquisition and post-analysis. Frequency analysis on AE signals can be carried out independently after signal acquisition. Interference among different functions is effectively avoided while data streaming is continued. In the acquisition software, pre-set trigger threshold is utilized to recognize AEs from background noises. Normally, threshold level is manually set by evaluating temporal background noise level. Herein, it is set to be 0.01V which is slightly beyond the background noise level. After being triggered, 8,000 points data lengths (0.2 μs time interval) can be recorded with 30% pre-trigger data points. Therefore, FFT resolution would be 625 Hz, which is adequate for frequency content analysis. The software profile can simultaneously display 8-channel signal waveforms fetched and traditional AE parameter diagrams such as accumulated event number (AEN) and event rate (ER) in real time. All signals are stored for post-analysis.

3. Experimental setup

3.1 Cubic-splitting test

The objective of cubic-splitting test was to induce a tensile crack dominant failure on mortar
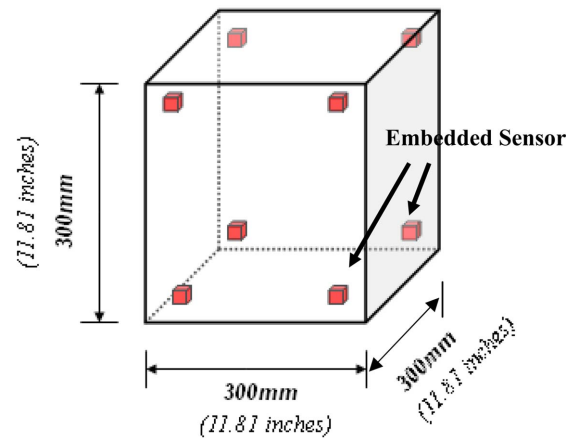
Fig. 3 Layout of embedded sensors array in cubic-splitting test
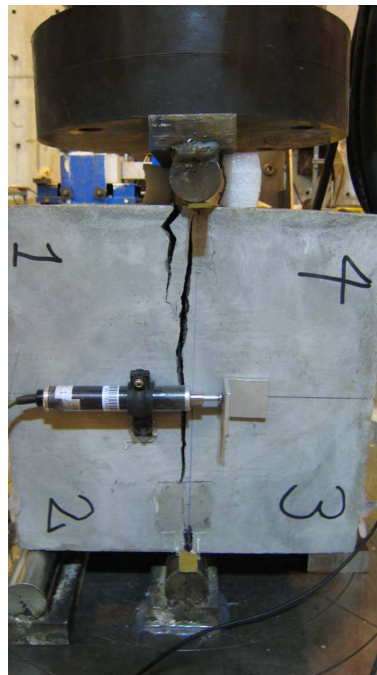

Fig. 4 Experimental setup and failure mode of cubic-splitting test

specimen (see Fig. 4). And the generated AE signals during the test were collected to investigate the frequency content characteristics of corresponding fracture process. The test procedure and apparatus were designed according to ASTM C496-96, while the adopted dimension of mortar specimen was a 300 mm*300 mm*300 mm (11.81 in.*11.81 in. *11.81 in.) cube with sensors embedded in the eight corners to form a detection array (see Fig. 3). Specimens (in cubic-splitting, direct-shear and pull-out tests) were prepared using mixture proportions of 1:0.5:1.8 (cement: water: sand) with 0.2% superplasticizer.

Two LVDTs of 10 mm (0.394 in.) working range were mounted on the front and back side of the
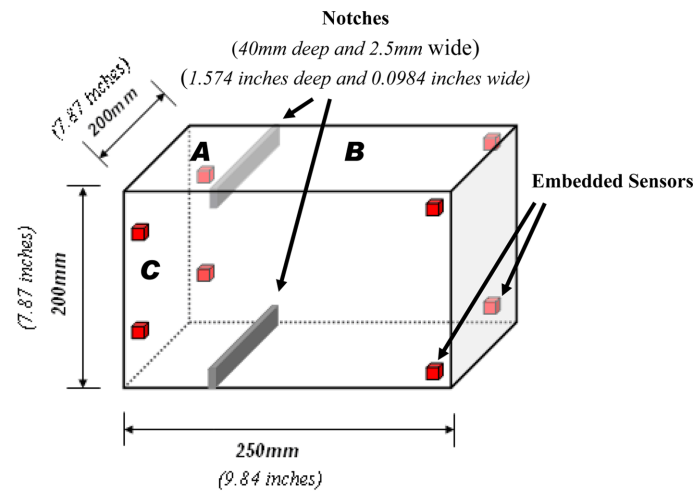
Fig. 5 Layout of embedded sensors array in direct-shear test

mortar cube in horizontal direction to measure the horizontal relative displacement due to expansion. A feedback mode control was applied to guarantee a stable loading process. When compressive force is applied on the top and bottom center line of the specimen, micro-cracks are expected to gradually occur in the region with high tensile stress. All micro-cracks and macro-cracks were expected to be detected by the embedded cement-based piezoelectric sensors array.

3.2 Direct-shear test

The objective of direct-shear test was to produce a shear mode fracture process on mortar specimen (see Fig. 6). Similarly, the AE signals generated were fetched for frequency content

Fig. 6 Experimental setup and failure mode of direct-shear test

analysis. ASTM standard D5607-02 (Standard Test Method for Performing Laboratory Direct Shear Strength Tests of Rock Specimens under Constant Normal Force) was used as reference for apparatus and test procedure design. The specimen was a 250 mm (9.84 in.) long, 200 mm (7.87 in.) wide and 200 mm (7.87 in.) high prism. A 40 mm deep and 2.5 mm wide notches were introduced in both the top and bottom regions of the prism with a distance of 50 mm from surface C (see Fig 5). The layout of cement-based piezoelectric sensors array was slightly different from the rest of the tests due to the presence of induced notches. Right hand side sensors (supposed to be embedded in the corners) were actually kept a distance of 40 mm (1.57 in.) vertically from the top or bottom surfaces for safety and reliability reasons (see Fig. 5). The experimental setup for direct-shear test is shown in Fig. 6. Cracks were expected to be initiated at the tip of the introduced upper notch of the prism, and propagate roughly along the negative direction of Y axis (downwards) when push-down force was applied on surface A. The rest of the prism was tightly restricted by a couple of flat steel plates clamped by four high yield steel bars. LVDTs of 25 mm (0.984 in.) working range were installed on the top of the mortar prism to record the vertical downward displacement of surface A relative to the stationary reference plate (surface B). Similarly, a good feedback mode control was employed.

3.3 Pull-out test

The objective of pull-out test was to produce a gentle debonding process between mortar and embedded round steel bar for AE analysis. The dimension of mortar specimen and layout of cement-based piezoelectric sensors array were identical to that of cubic-splitting test (see Fig. 7). A 16 mm (0.63 in.) diameter plain round steel bar was embedded into the mortar specimen with a depth of 200 mm (7.87 in.) during mortar construction (see Fig. 7). A couple of high stiffness steel plate was employed to fix the position of mortar cube during pull-out test. Experimental set-up for
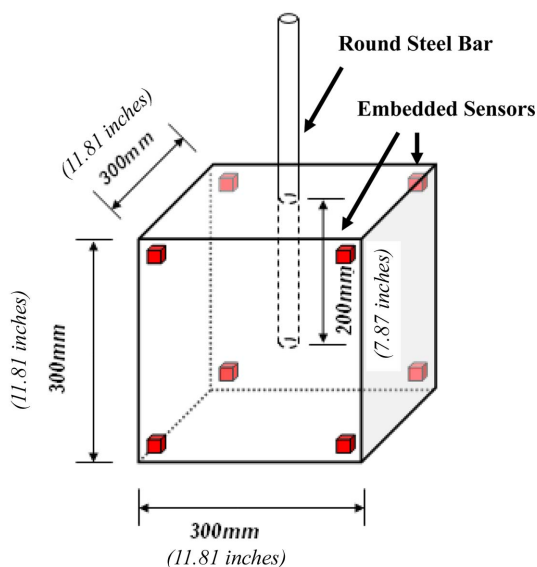

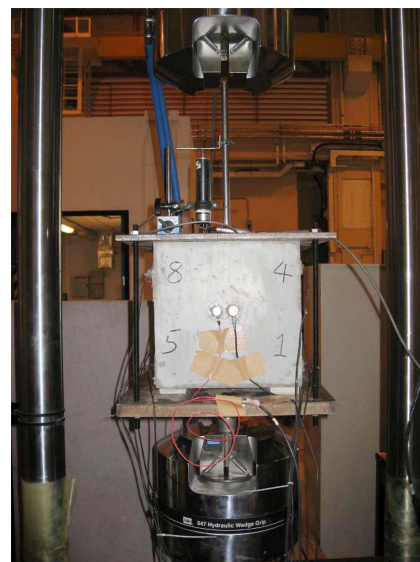Fig. 7 Layout of embedded sensors array in pull-out test

Fig. 8 Experimental setup of pull-out test

pull-out test is illustrated in Fig 8. The steel bar was fixed by clamp of MTS machine while the mortar cube was pulled down by actuator through loading fixture during the test. Based on simulation, debonding failure was expected to occur on the interface of mortar and embedded steel bar when a sufficient pull-out force was applied. LVDTs of 25 mm (0.984 in.) working range were installed on the top side of the mortar cube to measure the vertical displacement of the steel bar relative to the stationary reference plate of the apparatus. Feedback mode control was applied to guarantee the stability of loading process.

4. Parameter-based AE analysis

4.1 Cubic-splitting test

The fracture process of mortar cube in cubic-splitting test can be illustrated by corresponding AE parameters in Figs. 9 and 10. Given variation characteristics of AE parameters (i.e., AEN and ER), the entire fracture process is divided into four major regimes denoted as A B C and D. It can be seen from Fig. 9 that before 33.9% of ultimate load, almost no AE was detected. Thus, no detectable mortar cracks occurred in regime A. Between 33.9% to approximately 84.7% of ultimate load, fracture stage commences to enter pre-burst region featured by a small amount of AEN recorded and a slow ER (Lu and Li 2008). Although AE events occurred in regime B is relatively limited and stable, it is considered that micro-cracks started to accumulate in the mortar and caused the initial nonlinearity of load-deformation curve (Lu *et al*. 2010). Right after the moment when applied load level is over 84.7% of ultimate load, a significant large amount of AE events was collected abruptly in regime C. The corresponding time period is denoted as burst region featured by the significant rise of AEN recorded with a sharp rise slope and a fast ER (Lu and Li 2008). At this moment, a major crack quickly formed and propagated at the center of the specimen leading the
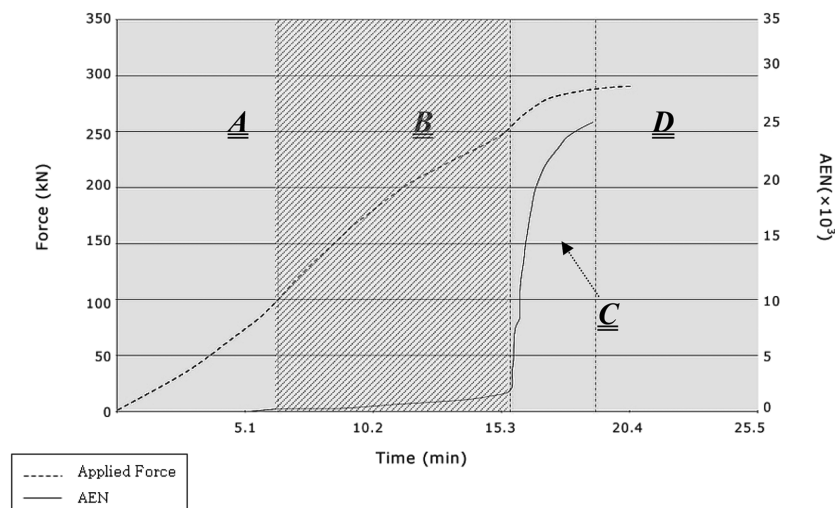

Fig. 9 Loading history & AEN diagram of cubic-splitting test (with dash dot lines indicating the regime boundaries)
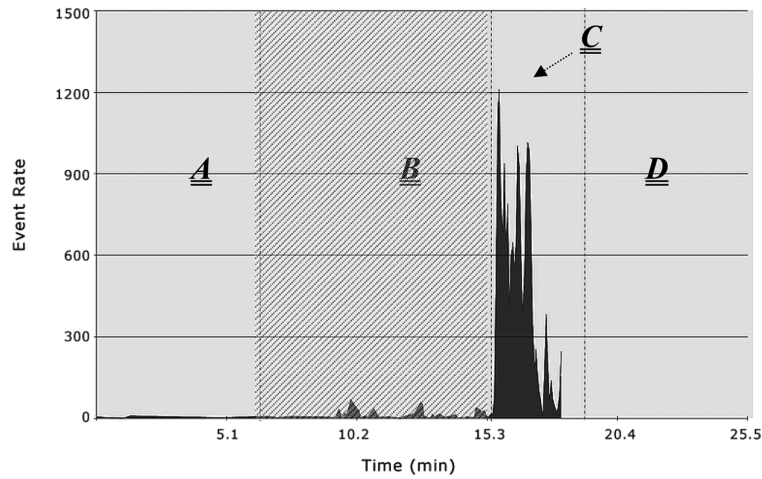
Fig. 10 ER diagram of cubic-splitting test (with dash dot lines indicating the regime boundaries)

specimen to be split apart (see Fig. 4). Clearly, cubic-splitting of mortar belongs to a typical brittle fracture process.

4.2 Direct-shear test

Similarly, the fracture process of mortar prism in the direct-shear test can be illustrated by its corresponding AE parameter variations in Figs. 11 and 12. And the fracture process is divided likewise into four major regimes. In regime A, the specimen deforms essentially linear elastically prior to 38% ultimate load applied. AEs occur rarely, and applied load level at this moment was yet not able to induce detectable micro-cracks in mortar. In regime B, micro-cracks commence to occur and accumulate in mortar prism. Once 88.2% of ultimate load level is reached in regime C, an AE burst region can be clearly identified from the observed significant increase of AEN and ER. These
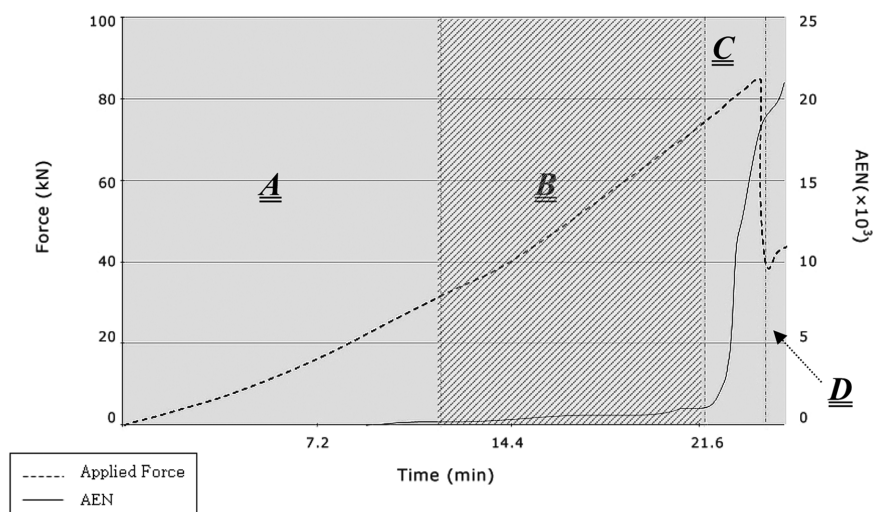

Fig. 11 Loading history & AEN diagram of direct-shear test (with dash dot lines indicating the regime boundaries)
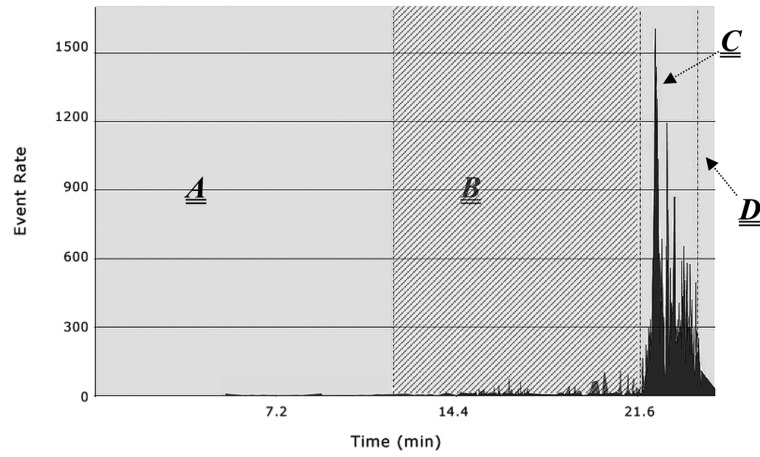
Fig. 12 ER Diagram of direct-shear test (with dash dot lines indicating the regime boundaries)

behavior characteristics of AE parameters indicate the transition from micro-cracks localization to major crack propagation, and fracture process of direct-shear test turns out to be brittle.

4.3 Pull-out test

The damage process of pull-out test is illustrated by the behavior analysis of AE parameters as well (see Figs. 13 and 14). Prior to 44% of ultimate load, seldom AE event can be observed. Apart from the induced elastic deformation, the applied load level in regime A is deemed yet not capable of producing evident debonding or micro-cracks. From 44% to 88.3% of ultimate load, AEs start to appear indicating that debonding and micro-cracks are considered to occur and develop during pull-out. Right after the moment when 88.3% of ultimate load is reached, both ER and AEN values
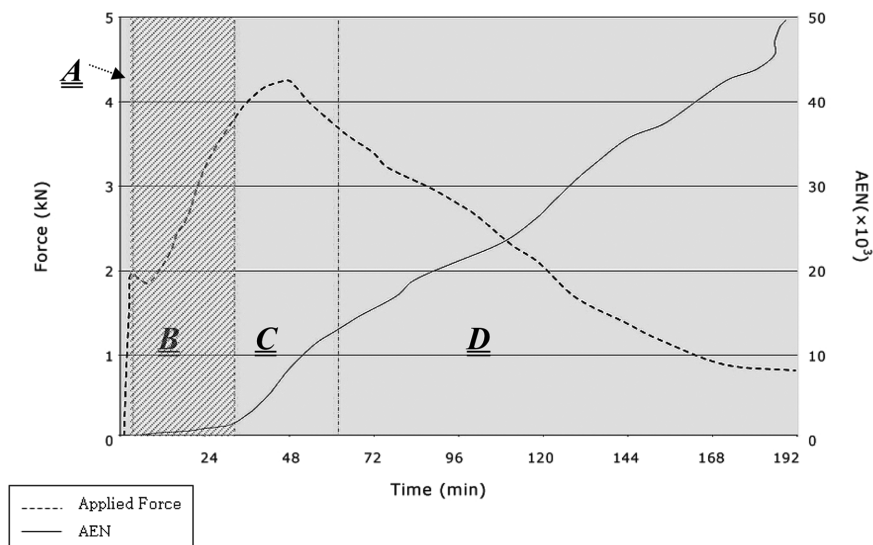

Fig. 13 Loading history & AEN diagram of pull-out test (with dash dot lines indicating the regime boundaries)
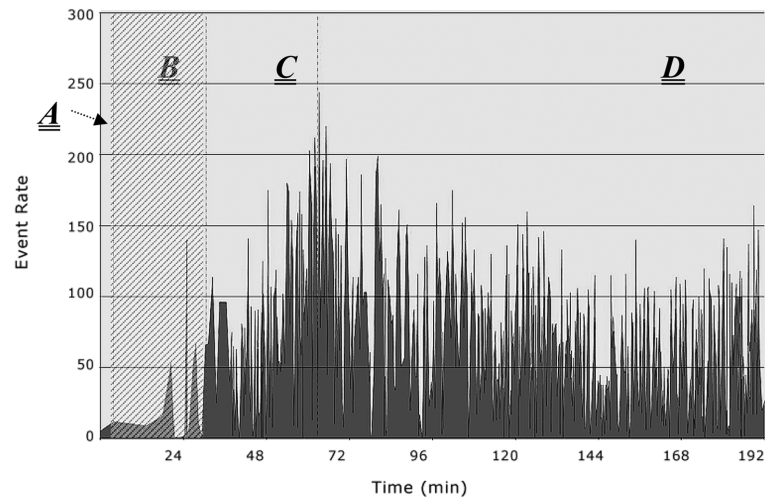
Fig. 14 ER diagram of pull-out test (with dash dot lines indicating the regime boundaries)

commence to increase rapidly with an obvious change in slope on AEN curve in Fig. 13. Debonding and micro-cracks become relatively more active in regime C. Compared to those of cubic-splitting test and direct-shear test, pull-out test turns out to be a relatively ductile process.

5. The frequency content of AE

The simplest form of AE recorded by sensor can be described by a factored exponential decaying sinusoidal function (Eq. (2)) as illustrated in Fig. 15 (Lu *et al.* 2010). Its corresponding frequency domain representation is a single sharp peak emphasizing the dominate frequency content contained
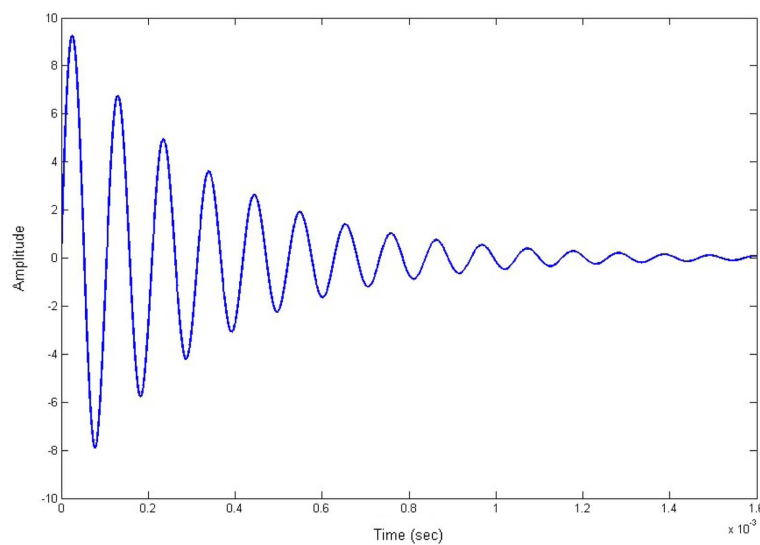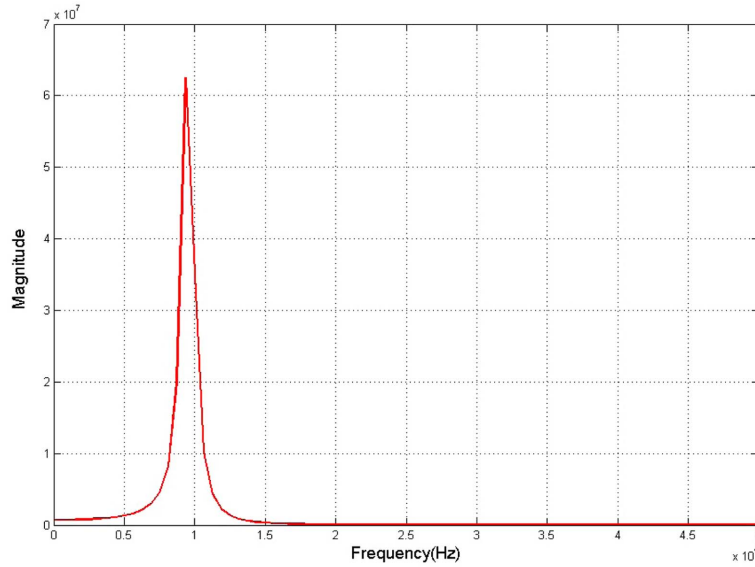

Fig. 15 A Simple AE Waveform

Fig. 16 Frequency domain response

(see Fig. 16).

$$f(t) = A_0 e^{-\alpha t} \sin(\omega t) \tag{2}$$

And Figs. 17-19 show the typical time domain waveforms and frequency domain power spectrums of AEs detected in cubic-splitting, direct-shear and pull-out test, respectively. In general, the major component in the time domain waveform of AE signal from concrete crack is superposition of a series of factored exponential decaying sinusoidal functions with various characteristic parameters regardless of applied loading patterns. Therefore, the corresponding frequency domain power spectrum diagrams always present the typical pattern of widely speared frequency components over a large frequency range with enormous peaks. The frequency components out of the range of 20 kHz~1 MHz are greatly attenuated by band-pass filters inside pre-amplifiers, and can be negligible. Hence, SNR is enhanced due to the reduction of noise level by the stop band of filters. The frequency content in spectrum diagrams can be regarded as the direct reflection of generated AE in frequency domain. Due to the
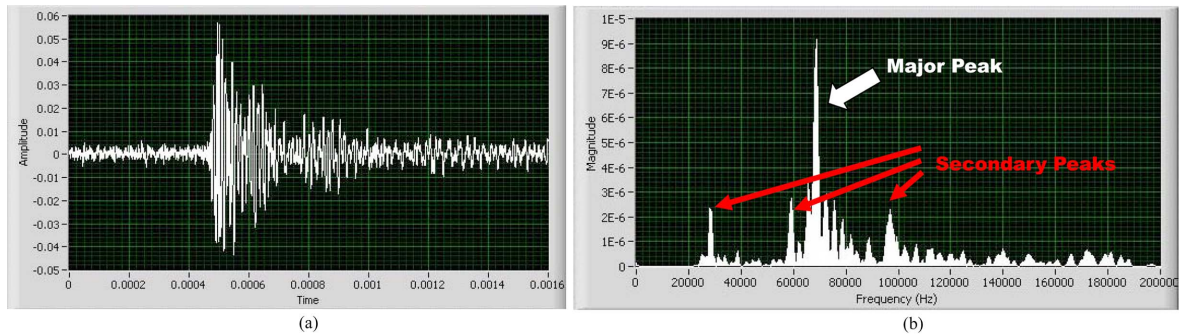

Fig. 17 (a) Waveform of a typical AE in cubic-splitting test and (b) frequency content of a typical AE in cubic-splitting test
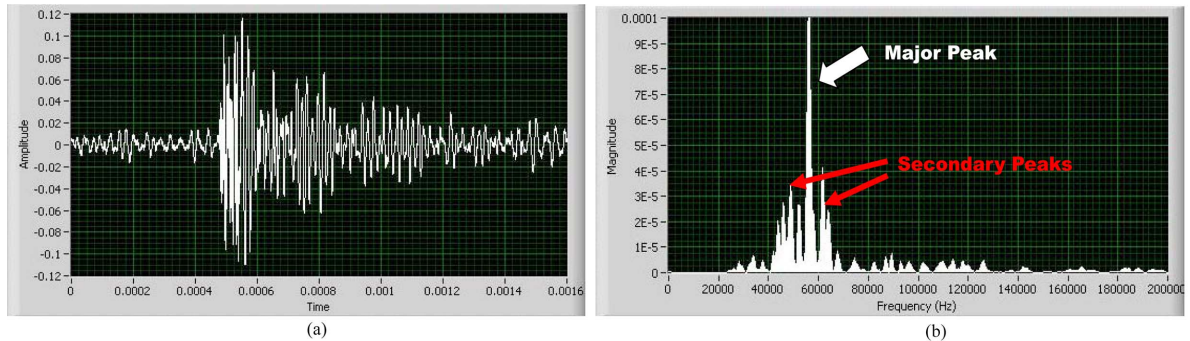
Fig. 18 (a) Waveform of a typical AE in direct-shear test and (b) frequency content of a typical AE in direct-shear test
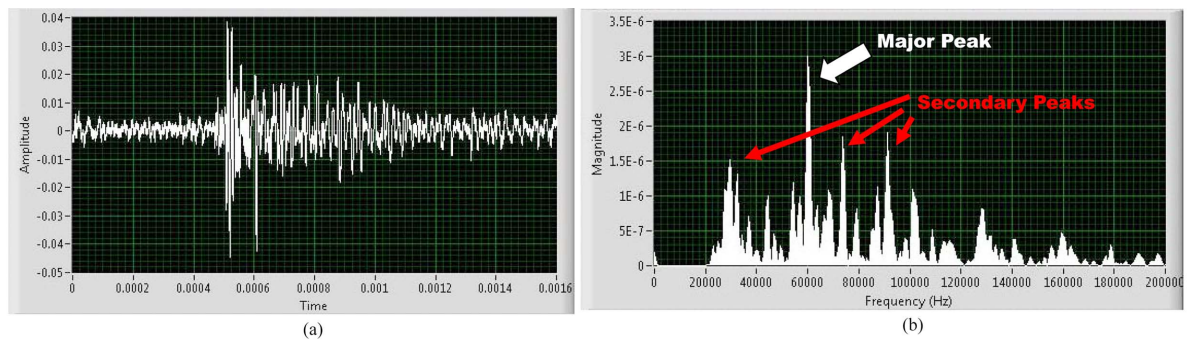

Fig. 19 (a) Waveform of a typical AE in pull-out test and (b) frequency content of a typical AE in pull-out test

possibly complex behavior of the AE sources (i.e., micro-crack of mortar) and the inhomogeneous character of concrete materials, it is reasonable to expect a typical scattered spreading style in their frequency domain response diagrams (Daponte *et al*. 1995). Whereas, among enormous peaks and valleys, a major peak can be clearly figured out in each frequency domain diagram, which exhibits the most significant frequency component contained in its corresponding exponential decaying sinusoidal function. And this frequency component is mostly found unique in the acquired AE with rare case of multiple comparable major peaks. This unique frequency component has a direct link with the local condition of its acoustic source, and can be utilized to reflect the major micro-crack behavior occurred at this source location. However, in reality, it is difficult and inaccurate to make judgments on the frequency content variations of AEs depending merely on eye observation due to the scattered spreading style of acquired AE frequency content and enormous quantity of acquired AE signals during fracture process. The frequency components contained in enormous secondary peaks should not be overlooked. Appropriate frequency content evaluation methods need to be utilized.

5.1 Spectral centroid

An effective way to characterize the variation tendency of AE frequency content is to calculate its spectral centroid (SC). Here, SC is short for the geometrical centroid of entire area embodied in frequency domain power spectrum diagram in linear scale, which is mathematically described in Eq. (3). Naturally, the variations of AE frequency content are able to be indicated by the variation of evaluated corresponding SC values.

$$SC = \frac{\sum_{n=0}^{N-1} f(n)x(n)}{\sum_{n=0}^{N-1} x(n)} \qquad (3)$$

$f(n)$ refers to the center frequency of the bin number n.
$x(n)$ represents the magnitude of the bin number n.

5.2 HL ratio

From literature, it is known that AEs from concrete fracture were reported mostly distributed in the frequency range of 20 kHz ~ 500 kHz (Li and Shah 1994, Maji and Sahu 1994, Ohtsu 1996, Tanigawa *et al.* 1980). Herein, based on the evaluation results of SC, the frequency content within the range of 80 kHz ~ 500 kHz is specified as the high frequency component contained in AE. Similarly, the frequency content within the range of 20 kHz ~ 80 kHz is conversely specified as low frequency component in AE. Their corresponding weights are evaluated according to the area below the spectrum curves within specified frequency range. The total energy of AE signal will be equal to the sum of energy contained in the specified frequency components according to Parseval's Theorem. It is expected that the ratio of the high component weight over low frequency one shall experience observable variations when there is a shift in the AE frequency content. Therefore, the defined HL ratio ϕ in Eq. (4) is regarded as an indicator of frequency content variation tendency.

$$\phi = \frac{\sum_{n=N_h}^{N_h^e} f(n)x(n)}{\sum_{n=N_l}^{N_l^e} f(n)x(n)} \qquad (4)$$

$f(n)$ refers to the center frequency of the bin number n.
$x(n)$ represents the magnitude of the bin number n.

Since the determination of high frequency range and low frequency range is sort of haphazardness, the evolution trend instead of absolute value in HL ratio is more meaningful in this study. And HL ratio based evaluation methods of AE frequency content shall be used together with according SC values to verify the obtained results on AE frequency content variation tendency.

6. AE frequency content analysis

Frequency domain analysis of the AE from concrete crack and various failure modes is currently considered as one of the most promising method to investigate the fracture process of concrete (Waenemuende and Wu 2004, Lamonaca and Corrozzini 2009 and Bocca *et al.* 2010). Given the direct physical link between acoustic source and the corresponding acquired AE signal as described in Eqs. (5) and (6), it is considered that micro-crack behavior of the concrete during loading process

would actively modulate the frequency content characteristics of generated AEs accordingly provided changeless propagation medium and monitoring system (Maji and Sahu 1994, Tanigawa *et al.* 1980).

$$V(t) = T(t)*[G(t)*M(t)] \tag{5}$$

Where $V(t)$ is the detected AE signal waveform function in time domain, $T(t)$ is the response function of the monitoring system, $G(t)$ is the elastodynamic Green's function for mortar, and $M(t)$ is a time domain function of the acoustic source. *denotes a convolution integral.

$$V(s) = T(s) \cdot [G(s) \cdot M(s)] \tag{6}$$

Eq. (6) represents the Laplace transform of Eq. (5) so as to illustrate the relationship between detected AE signal and acoustic source in S-domain. Provided that $S = j\omega$, frequency domain spectrum can be determined from Eq. (6) by variable substitution.

In this study, the frequency content evaluation methods stated previously were utilized to investigate the frequency content variation characteristics of AEs from concrete micro-cracks and damages. From parameter-based analysis of AE, it was observed that when the applied load level reached around 85% of ultimate load, micro-cracks started to burst out dramatically in cubic-splitting and direct-shear tests. This is known as micro-cracks localization period, and corresponds to AE burst region. It is the transition from distributed micro-cracks to major macro-cracks. After the ultimate load reached, AEs are generally considered to be contributed by macro-crack propagation and other associated mechanisms. During the micro-crack localization and following macro-crack development stage, cracks and damages commence to modulate the frequency content of detected AEs together with crack behavior due to the prevalent presence of cracks in their propagation paths. The relationship illustrated in Eq. (6) has to be appended with an additional function $K(s)$ reflecting temporal state of damage level. And this additional function is time-variant during the fracture process of mortar. Hence, in order to expressively study the frequency content characteristics of AE from concrete cracks, frequency content analysis was specially performed aiming at the period prior to AE burst region. That is AE pre-burst region highlighted in regime B of Figs. 9-14. Frequency content attribution due to the state change of propagation medium is thereby neglected. Since AE pre-burst region is an ER stable loading stage, the occurring rate of AE is approximately proportional to the applied loading rate. Thus, evaluation results were plotted in terms of AE event number instead
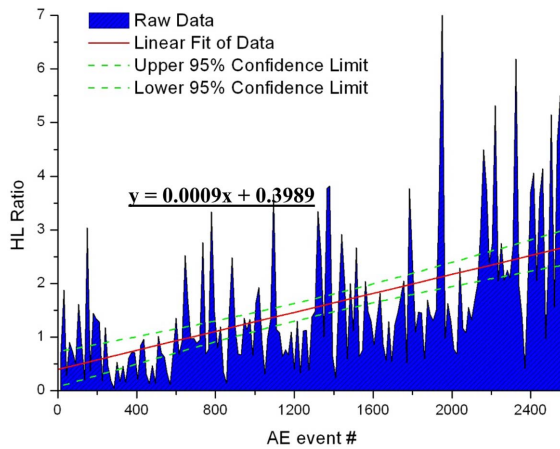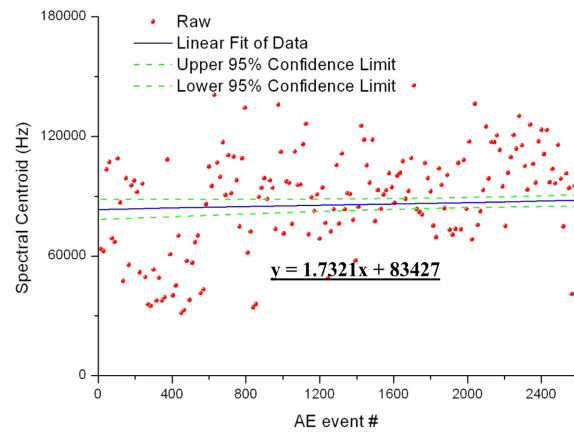

Fig. 20 HL ratio in cubic-splitting test
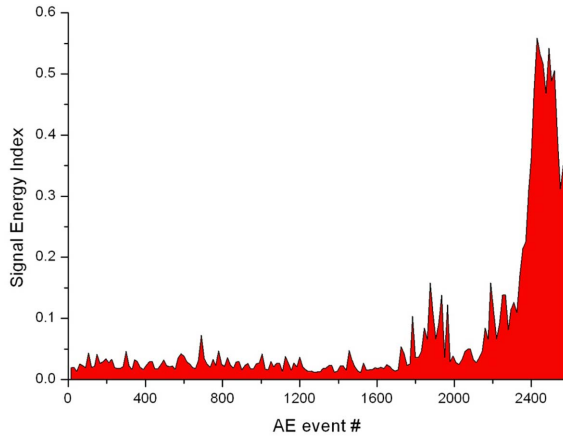

Fig. 21 SC in cubic-splitting test

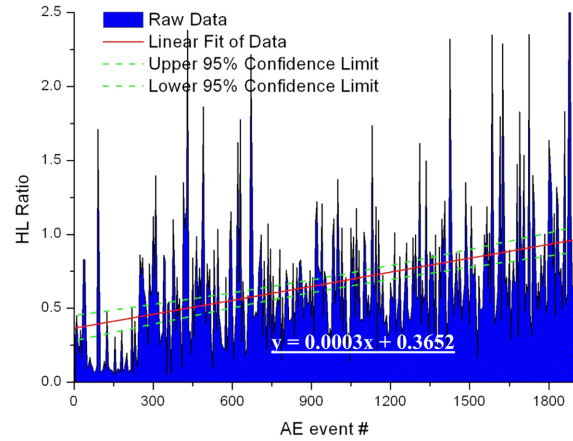Fig. 22 AE signal energy index in cubic-splitting test
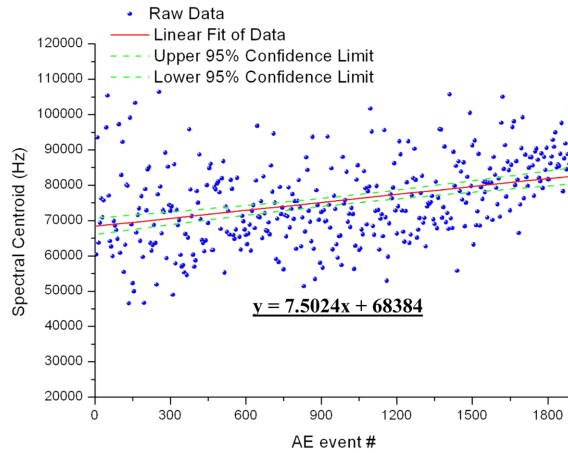

Fig. 23 HL ratio in direct-shear test
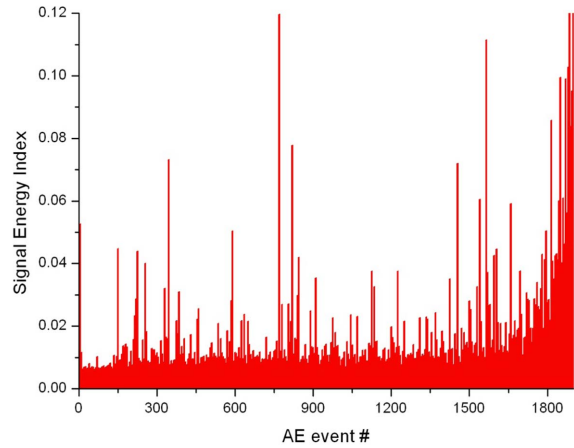

Fig. 24 SC in direct-shear test

Fig. 25 AE signal energy index in direct-shear test

of applied load level so as to clarify the variation of frequency content of AE acquired.

Figs. 20, 23 and 26 illustrate the variations of HL ratios evaluated from AE signals detected in regimes B of cubic-splitting, direct-shear and pull-out tests respectively. Although the ratio values exhibit evident scatter distribution style, an obvious rising trend can be figured out from the positive slopes of fitted linear equations highlighted in Figs. 20, 23 and 26. Simply speaking, the frequency content of AE signals in general shifts to higher range with the applied load level in regime B.

Results in Figs. 21, 24 and 27 verify the rising trends of AE signal frequency content within regimes B of cubic-splitting, direct-shear and pull-out tests. Despite of the different loading patterns, evaluated SC values of acquired AEs evidently shift to higher value gradually with the applied load level in regimes B. Without exception, positive slopes were obtained in all the fitted linear equations as highlighted in corresponding figures. However, the values of SC in pull-out test are mostly distributed in the range of 120 kHz~140 kHz, which is apparently higher than that of cubic-splitting and direct-shear tests. Since debonding is considered as dominant damage mechanism occurred during pull-out test, it is expect that the AE signals may own a distinct frequency domain power spectrum. Both of the frequency content evaluation methods reveal the factor that prior to the
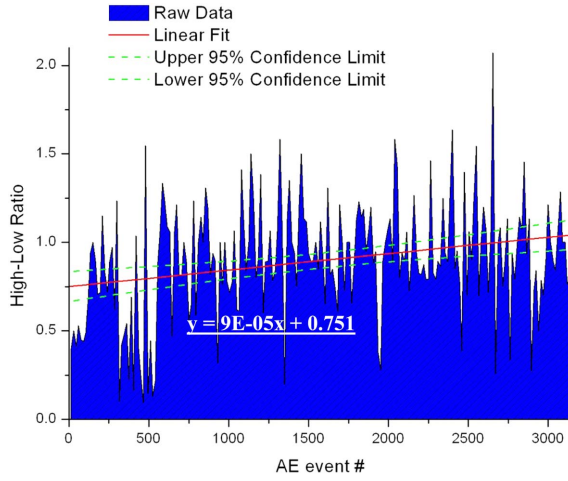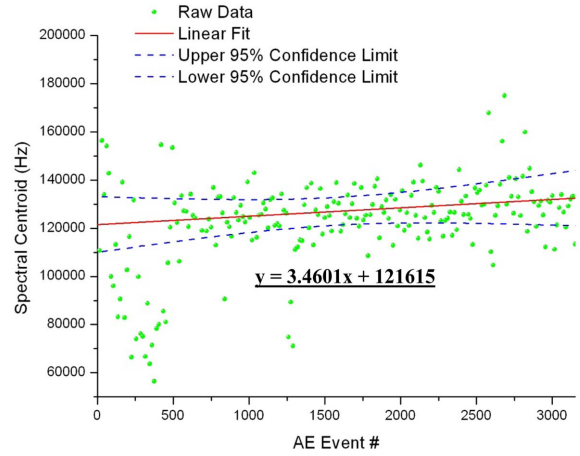
Fig. 26 HL ratio in pull-out test

Fig. 27 SC in pull-out test

micro-crack localization stages (e.g., AE pre-burst region), the frequency components of AE signals acquired in cubic-splitting, direct-shear and pull-out tests apparently shift to higher range hand in hand with the applied load levels. This phenomenon is consistent with the observation of Tanigawa *et al.* (1980).

7. AE energy index analysis

Physically, AE refers to the elastic wave generated when there is a rapid release of energy in a material. The released energy propagates in the form of elastic wave and turns into the kinetic energy and strain energy of local elements. And it had been proved that the kinetic and strain energies of the local elements at any instant were equal (Timoshenko and Goodier 1970). Therefore, consideration of either one is sufficient for evaluating the total energy released. Here for simplicity, the kinetic energy T of a local element can be described by Eq. (7).

$$T = \frac{1}{2}\rho dxdydz\left(\frac{\partial u}{\partial t}\right)^2 \tag{7}$$

ρ refers to the density of propagation medium.
u refers to motion displacement of local element.

It is revealed by Eq. (7) that AE energy is linear proportional to the sum of velocities of motion in local elements. After AE being detected by cement-based piezoelectric sensors, the velocities are converted to corresponding signal outputs according to sensor calibration response. Hence, it is feasible to evaluate the AE energy by estimating its corresponding acquired AE signal energy. Since AE signal is generally considered as a function of varying amplitude through time, it is appropriate to use the area involved in the waveform $f(x)$ enveloping curve as a good approximate measurement of the energy of an AE signal. Hence, the total energy of a signal $f(x)$ can be represented in Eq. (8).
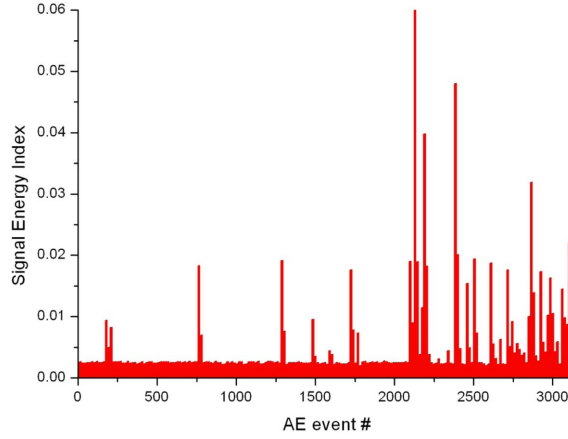
Fig. 28 AE signal energy index in pull-out test

$$\|f(x)\|^{\Delta} \; = \; \sqrt{\varepsilon} \; = \; \sqrt{\sum_{x=0}^{N-1} |f(x)|^2} \tag{8}$$

x refers to the discrete time point of the detected signal.
N represents the total number of the discrete time points.

The $\|f(x)\|$ can be considered as the length of the vector $f(x)$ in N-space, and as the absolute value or radius of a vector to scale the AE energy released during damage process. In fact, it is not a dimensional physical quantity of AE energy released but a customized index. Figs. 22, 25 and 28 reveal the AE signal energy index for the cubic-splitting, direct-shear and pull-out tests. Based on the direct relationship existed between AE signal energy and fracture energy (Prasad and Sagar 2008, Landis and Baillon 2002), evaluated AE signal energy index can be utilized to quantitatively represent the fracture energy released by corresponding micro-crack. Given that the damage level of mortar in AE pre-burst region is not severe yet, estimated energy attenuation of the AE signals due to the presence of mortar micro-cracks can be considered very limited. Therefore, the effect of existed damage is considered hardly noticeable in this study. Comparisons on evaluated absolute values make little sense since evaluated index is a multivariable function of both micro-crack behavior and propagation trajectory. Herein, evaluated AE signal energy index was utilized as the indication of the micro-crack magnitude variation during the tests. From those figures, it is seen that the energy indices within the majority of AE pre-burst region stay in a stable level, revealing that magnitudes of micro-cracks are relative stable prior to the micro-cracks localization period regardless of loading patterns. It can be seen that AE signal energy indices present little sign of increasing until fracture processes are close to the specified AE burst region. Big cracks or linkage of existed mass of micro-cracks seem to appear at this moment, which is represented by the significant increase of the energy indices.

Based on the comparison between corresponding AE frequency content and signal energy index variation characteristics, it is found that they exhibit different variation tendencies prior to AE burst region in cubic-splitting, direct-shear and pull-out tests. Basically, frequency content owns an obvious trend of shifting to higher frequency range, while energy indices keep stable until the very end of regime B. Nevertheless, there exists a deep relationship between energy and frequency spectrum.

Essentially, frequency domain power spectrum of AE shown previously is kind of way illustrating the energy distribution in frequency domain. Frequency content magnitude can be regarded as the relative weight of signal components within corresponding frequency range contained in each AE signal. Thus, high frequency signals thereby belong to a sort of signals owning more energy weight in high frequency range. And the shift of frequency content is considered to be the direct consequence of the shift of signal spectral energy. Herein, during AE pre-burst regions of cubic-splitting, direct-shear and pull-out tests, high frequency components apparently occupy more and more weight of energy continuously in each AE signals with the applied load level. While the magnitudes of micro-cracks stay the same. Therefore, the observed variation in frequency content is a direct result of the change in micro-crack behavior instead of micro-crack magnitude of acquired AE as described in Eq. (6). Study on crack mode classification based on AE showed that the loading stages of concrete under uniaxial tension seemed to be accompanied by variation of dominant crack modes (Li 1996, Landis and Shah 1993). The angle between the micro-cracks and Burger tensors were found exhibiting an obvious tendency of increasing prior to major crack development. Despite of the factor that most of AEs acquired belong to mixed mode micro-crack, the results of motion direct angle respect to micro-crack plane apparently reveal that micro-crack behavior variation continuously underwent during the tests. These findings imply that a close relationship may exist between the variations of crack modes and evaluated frequency content of corresponding AEs during the fracture process. The observed variation characteristics in the frequency content of AEs can possibly reflect the variation characteristics of crack mode during the loadings.

However, the study on the variation characteristics of AE frequency content after micro-cracks localization period is not included since the presence of existed cracks along the path of AE propagation will cause an inestimable effect on the frequency components of AE generated. Daponte *et al.* stated the existed micro-cracks or damages would increase the inhomogeneity of mortar, and consequently caused AE energy to spread from a centralized frequency range to a wider range. Thus the variation characteristics of frequency content due to micro-crack behavior will be diluted. Therefore, an appropriate manner is needed for further evaluation of frequency content of AE from mortar after AE burst.

8. Conclusions

Frequency domain analysis on AE from concrete fracture is of great interest for deep exploration of concrete crack behavior. Towards this end, frequency content characteristics of AEs from mortar were investigated using improved AE monitoring system. Cement-based piezoelectric sensor featured broad band frequency domain response and high sensitivity was employed in the tests to perform AE monitoring. The corresponding variation tendencies of frequency content were evaluated by means of the defined HL ratio and SC value. Meanwhile, AE signal energy index was utilized to investigate the magnitude of micro-crack energy evolution during the tests. It is found the frequency content has a trend of shift to higher range with the applied load level, while AE energy remains in a stable level until the fracture processes approached AE burst region in cubic-splitting, direct-shear and pull-out tests. Based on literature and analysis, it is revealed that the variation characteristics of AE signals have a close relationship with the variation of micro-crack behaviors during the fracture processes of mortar. Frequency content of AE has a great potential to be utilized as a useful tool for monitoring and investigating temporal micro-crack behavior of mortar.

Acknowledgements

References

Akdogan, E., Allahverdi, M. and Safari, A. (2005), "Piezoelectric composites for sensor and actuator applications", *IEEE T. Ultrason. Ferr.*, **52**(5), 746-775.

Berthelot, J., Souda, M. and Robert, J. (1992), "Frequency response of transducers used in acoustic emission testing of concrete", *NDT & E Int.*, **25**(6), 279.

Bocca, P., Lacidogna, G., Grazzini, A., Manuello, A., Masera, D. and Carpinteri, A. (2010), "Creep behavior in reinforced masonry walls interpreted by acoustic emission", *Key Eng. Mater.*, **417-418**, 237-240.

Carpinteri, A., Lacidogna, G. and Pugno, N. (2007a), "Structural damage diagnosis and life-time assessment by acoustic emission monitoring", *Eng. Fract. Mech.*, **74**(1-2), 273-289.

Carpinteri, A. and Lacidogna, G. (2007b), "Damage evaluation of three masonry towers by acoustic emission", *Eng. Struct.*, **29**(7), 1569-1579.

Daponte, P., Maceri, F. and Olivito, R. (1995), "Ultrasonic signal-processing techniques for the measurement of damage growth in structural materials", *IEEE T. Instrum. Meas.*, **44**(6).

Grosse, C., Reinhardt, H. and Finck, F. (2003), "Signal-based acoustic emission techniques in civil engineering", *J. Mater. Civil Eng.*, **15**(3).

Lamonaca, F. and Carrozzini, A. (2009), "Nondestructive monitoring of civil engineering structures by using time frequency representation", *Proceedings of the IEEE International Workshop on Intelligent Data Acquisition and Advanced Computing Systems: Technology and Applications*, Rende, Italy, September.

Landis, E. and Baillon, L. (2002), "Experiments to relate acoustic emission energy to fracture energy of concrete", *J. Eng. Mech.*, **128**(6).

Landis, E. and Bolander, J. (2009), "Explicit representation of physical processes in concrete fracture", *J. Phys. D. Appl. Phys.*, **42**(21), 214002, 17.

Landis, E. (1999), "Micro-macro fracture relationships and acoustic emissions in concrete", *Constr. Build. Mater.*, **13**(1-2), 65-72,1999.

Landis, E. and Shah, S. (1993), "Recovery of microcrack parameters in mortar using quantitative acoustic emission", *J. Nondestruct. Eval.*, **12**(4), 219-232.

Li, Z. and Shah, S. (1994), "Localization of micro-cracking in concrete under uniaxial tension", *ACI Mater. J.*, **91**(4).

Li, Z., Zhang, D. and Wu, K. (2002), "Cement-based 0-3 piezoelectric composites", *J. Am. Ceram. Soc.*, **85**(2), 305-313.

Li, Z. (1996), "Microcrack characterization in concrete under uniaxial tension", *Mag. Concrete Res.*, **48**(176), 219-228.

Lu, Y. and Li, Z. (2008), "Cement-based piezoelectric sensor for acoustic emission detection in concrete structures", *Proceedings of the 11th International Conference on Engineering, Science, Construction, and Operations in Challenging Environments*.

Lu, Y., Li, Z. and Liao, W. (2010), "Damage monitoring of reinforced concrete frames under seismic loading using cement-based piezoelectric sensor", *Mater. Struct. RILEM*.

Maji, A. and Sahu, R. (1994), "Acoustic emission from reinforced concrete", *Exp. Mech.*, **34**(4), 279.

Ohtsu, M., Shigeishi, M., Iwase, H. and Koyanagit, W. (1991), "Determination of crack locations, type and orientation in concrete structures by acoustic emission", *Mag. Concrete Res.*, **43**(155), 127-134.

Ohtsu, M. (1996), "The history and development of acoustic emission in concrete engineering", *Mag. Concrete Res.*, **48**(17), 321-330.

Ohtsu, M. (1987), "Mathematical theory of acoustic emission and its application", *J. Soc. Mater. Sci.*, **36**(408),

1025-1031.

Prasad, B. and Sagar, R. (2008), "Relationship between ae energy and fracture energy of plain concrete beams: experimental study", *J. Mater. Civil Eng*., **20**(3).

Qin, L., Lu, Y. and Li, Z. (2010), "Embedded cement-based piezoelectric sensors for AE detection in concrete", *J. Mater. Civil Eng*., **22**(12), 1323.

Tanigawa, Y., Yamada, K. and Kiriyama, S. (1980), "Frequency characteristics of acoustic emission waves of concrete", Transactions of the Japan Concrete Institute, 2.

Timoshenko, S. and Goodier, J. (1970), *Theory of elasticity*, McGraw-Hill Book Co.

Warnemuende, K. and Wu, H. (2004), "Actively modulated acoustic nondestructive evaluation of concrete", *Cement Concrete Res*., **34**(4), 563-570.

BS